Degrees of Freedom With Small and Large Linear Surfaces in the Near Field

Athanasios G. Kanatas*, Harris K. Armeniakos*, and Harpreet S. Dhillon+
*Department of Digital Systems, University of Piraeus, Piraeus, Greece
+Bradley Department of Electrical and Computer Engineering, Virginia Tech, Blacksburg, VA, 24061, USA
Email: {harmen,kanatas}@unipi.gr, hdhillon@vt.edu

***Abstract*—This paper examines the number of the communication modes, i.e., the degrees of freedom (DoF), that are available in a wireless setup with a small linear intelligent surface in the near field of a large linear intelligent surface. The framework allows for any orientation between the surfaces and any position in a two dimensional space assuming that the transmitting one is placed at the origin. Therefore, apart from the length of the two surfaces, four more parameters are considered, the Cartesian coordinates of the center of the receiving surface and two angles that model each surface rotation around its center. The paper starts with the deterministic calculation of the DoF for a generic geometric setup, which extends beyond the widely studied paraxial setting. Subsequently, a stochastic geometry framework is proposed to study the statistical behaviour of the DoF under a typical geometric setup in a mmWave network. Numerical results revealed the extreme capabilities in the achievable DoF provided by near-field communications and allow the derivation of key system-level insights for mmWave 6G networks.**

***Index Terms*—Communication modes, degrees of freedom, holographic surfaces, intelligent surfaces, near field, stochastic geometry.**

I. Introduction

One of the promising technologies for 6G communications is the holographic multiple-input multiple output (HMIMO) surfaces [1]. These are reconfigurable intelligent surfaces of finite dimensions that can be treated as continuous arrays of infinite number of infinitesimal antennas [2], capable of controlling the radio environment in their proximity to some degree [3]. The need for understanding the achievable fundamental limits of these continuous intelligent surfaces in terms of orthogonal spatial communication modes is well recognized [4].The number of these modes, termed degrees of freedom (DoF), and the coupling intensity for two communicating surfaces are two of the foundational performance indicators of electromagnetic information theory (EIT) [5]– [7].

The increasing interest in these large surfaces along with the relevance of higher frequencies, such as millimeter wave (mmWave) in the current 5G systems and the sub-THz in the future 6G systems, is expected to result in a significant departure from the well-understood far-field regime to the less-explored near-field region, which is of interest to this paper [8]. Depending on the carrier frequency and the surface dimensions, the near field region can extend from tens to hundreds of meters. The boundary between the near-field and the far-field region can be tens or hundreds of meters. Consequently, unlike the traditional wireless generations, the future 6G systems will introduce links in the near-field where spherical wave models should be used. The novel opportunities for beam focusing, in contrast to the beam steering available in the far-field, will provide new capabilities in terms of signal processing and DoF [9]. Naturally, the analysis of key characteristics, such as DoF, require careful consideration of the distance relative to the surfaces dimensions and the relative geometry of the surfaces. Thus, when the paraxial approximation that is widely adopted is not fulfilled, i.e., the surfaces are not parallel and the distance is comparable to the surface dimensions, then the definition of the communication modes and the calculation of the DoF is not straightforward, and alternative methods are required. In [10], the authors have provided closed-form solutions for the case of a linear large intelligent surface (LIS) and a linear small one (SIS), which is of practical interest since it models the link between a base station and a mobile station. While this is a key step towards gaining a complete understanding of this regime, this work considered a limited geometric setup and the solutions were restricted to specific conditions.

Triggered by the aforementioned, in this work we develop a new analytical framework for calculating the DoF for the link between a LIS and a SIS that goes *beyond the paraxial setup*. We model the surfaces as ideal electromagnetic apertures in free space obeying the Huygens-Fresnel principle with a holographic capability. *Without putting any restrictions on the relative positions or orientations of the two array*s, we solve the underlying geometric problems to provide the required parameters for the calculation of the available communication modes. Further, to our knowledge this is also the first paper to explore the *statistical behaviour of the DoF* for a practical geometric setup under a stochastic geometry-based framework.

II. System Model

Consider two linear surfaces as shown in Fig. 1, where the origin of the reference system coincides with the center of the transmitting surface, with the x axis oriented in the horizontal and the y axis in the vertical direction. The transmitting surface, Tx, is a SIS. It has a length L_T and is rotated by an angle θ_T with respect to y axis, considering a positive angle for counterclockwise rotation and $-\pi < \theta_T \leq \pi$. The endpoints of the surface are denoted as T^+ and T^-. The

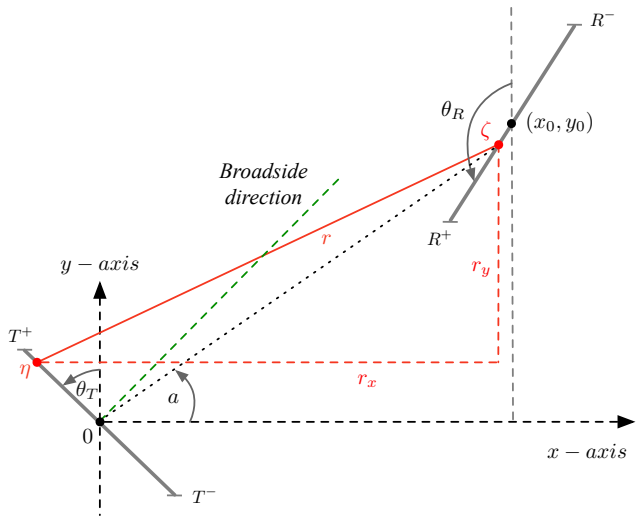

Fig. 1: The system model.

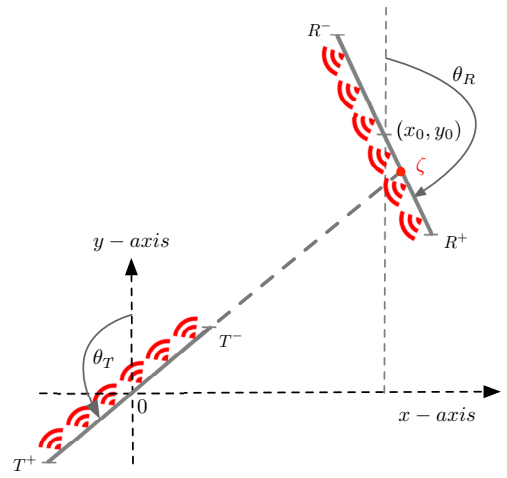

(a) The Rx is intersected

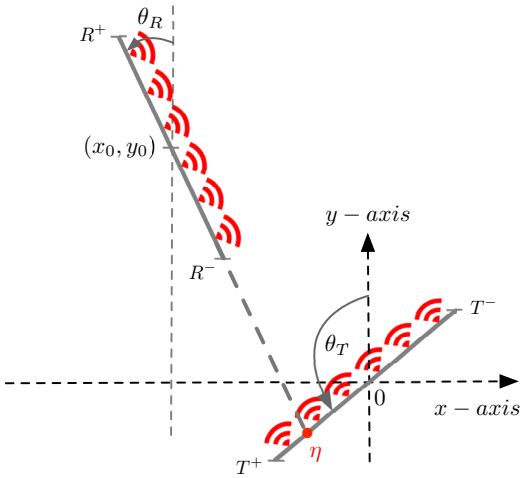

(b) The Tx is intersected

Fig. 2: Two indicative cases with intersections

receiving surface, Rx, is a LIS of length L_R, its center is located at (x_0, y_0), and is rotated by an angle θ_R with respect to y axis considering a positive angle for counterclockwise rotation and $-\pi \leq \theta_R \leq \pi$. The endpoints of the Rx surface are denoted as R^+ and R^-. Both surfaces are assumed lying on the same plane. Moreover, quite reasonably, we assume that both surfaces radiate only in one of the two half planes. Let η, $-L_T/2 \leq \eta \leq L_T/2$, denote the coordinate along the transmitting surface and ζ, $-L_R/2 \leq \zeta \leq L_R/2$, along the receiving surface with upward positive direction when $\theta_T = 0^o$ and $\theta_R = 0^o$, respectively. Thus, the coordinates of the two points are $(\eta \sin\theta_T, \eta\cos\theta_T)$ and $(\zeta\sin\theta_R, \zeta\cos\theta_R)$, respectively. The distance r between two points η and ζ on the two surfaces is given by

$$r = \sqrt{r_x^2 + r_y^2} = \sqrt{(x_0 + \eta\sin\theta_T - \zeta\sin\theta_R)^2 + (y_0 - \eta\cos\theta_T + \zeta\cos\theta_R)^2}. \quad (1)$$

Since in the considered model the receiving surfaces may be located anywhere on the plane and the two surfaces may be rotated, there is a possibility that the receiving side of one surface is not visible in its whole length from the transmitting side of the other surface and vice versa. Two indicative cases with partial visibility are depicted in Fig. 2. Therefore, based on the values of $x_0, y_0, \theta_T, \theta_R$ one should calculate the visible length of the two surfaces l_T, l_R respectively, as well as the points of intersection of the surfaces, denoted as η and ζ accordingly. Based on the location of these points one may calculate the new centers η_c, ζ_c of the two effective surface segments, respectively, and replace η with $(\eta+\eta_c)$ and ζ with $(\zeta+\zeta_c)$ in (1). Then, $-l_T/2 \leq \eta \leq l_T/2$, $-l_R/2 \leq \zeta \leq l_R/2$.

There are three more useful angles to be defined for each surface that will facilitate the calculation of the available DoF. The angles a_+, a_-, a_0, all in $(-\pi, \pi]$, denote those angles measured from the center of the transmitter to the two endpoints $L_R/2$, $-L_R/2$, and the center of the receiver, respectively. The reference zero value is measured from the local x axis through the center of the transmitting surface.

Based on a holographic assumption and a continuous phase profile with η, one may define a focusing function at the transmitting surface to focus the energy at the point ζ on the receiving surface, as

$$F_T(\eta)|_\zeta = \text{rect}\left(\frac{\eta}{l_T}\right) e^{j\frac{2\pi}{\lambda}r(\eta)}. \quad (2)$$

If the Taylor series expansion is used at $\eta = 0$ and if one keeps only two terms of the series, then

$$r(\eta) \approx r(0) + (\eta)\frac{\partial r(\eta)}{\partial \eta}\bigg|_{\eta=0}. \quad (3)$$

The number of the terms of the series to be kept is defined by the length of the transmitting surface, when the variables l_R, θ_T, θ_R, and x_0, y_0 are fixed. When two terms are kept the distance is approximated as a linear function of η. Using (1) the distance is written as

$$r(\eta) \approx r(0) + \eta\,\rho = r(0) + \eta\,\frac{\sin\theta_T - \gamma\cos\theta_T}{\sqrt{1+\gamma^2}}, \quad (4)$$

where

$$\gamma = \frac{y_0 + \zeta\cos\theta_R + \zeta_c\cos\theta_R - \eta_c\cos\theta_T}{x_0 - \zeta\sin\theta_R - \zeta_c\sin\theta_R + \eta_c\sin\theta_T} = \tan a, \quad (5)$$

and a is the angle formed by the segment from the center of the transmitter, η_c, to the point ζ and the x axis (see Fig. 1). If one keeps only the terms that depend on η and drop the terms that are independent of η, which contribute a constant phase shift to the focusing function, then

$$F_T(\eta)|_\zeta = \mathrm{rect}\left(\frac{\eta}{l_T}\right) e^{j\frac{2\pi}{\lambda}\rho\eta}. \quad (6)$$

Thus, the approximation in (4) results in a linear phase with η and consequently a beam steering phase profile and not a focusing one. This means that the Tx surface concentrates the energy towards the direction of the focal point in the far-field and is not capable of focusing. However, since the Rx surface is a large one, the Tx surface is in its near field and an increased number of modes is possible. Moreover, due to the reciprocity of the radio link, the DoF is the same if one switches the role of the two surfaces from Tx/Rx to Rx/Tx. Therefore, there is no need to examine separately the uplink and the downlink cases as far as the DoF is considered, as long as the definition of the orthonormal basis functions remains consistent.

III. Geometric Conditions for Visibility

The first geometric conditions to be examined refer to the mutual visibility of the two surfaces. As already explained, the receiving surface may be located anywhere on the plane. However, in practice its position, (x_0, y_0), may be confined in a circular disk of radius R. The radius depends upon the line-of-sight (LoS) restriction between the transmitter and the receiver. The two surfaces may be rotated and this affects their mutual visibility. The rotation is governed by the two angles θ_T, θ_R and depending upon the location of the Rx surface, there are four states: i) no visibility, ii) full mutual visibility, iii) the full length of the transmitter is visible from the receiver but the prolongation of the transmitting surface intersects the receiving surface, which is shown in Fig. 2a, and iv) the full length of the receiver is visible from the transmitter but the prolongation of the receiving surface intersects the transmitting surface, which is shown in Fig. 2b. For the last two states one should calculate the point of intersection, then identify the length of the surface $l_{T,R}$, that corresponds to the visible part, i.e., identify whether the visible part is from the point of intersection to $L_{T,R}/2$ or to $-L_{T,R}/2$, and finally calculate the center of the visible surface part ζ_c or η_c. The point of intersection at the Rx surface is calculated as

$$\zeta = \frac{x_0\,\cos(\theta_T) + y_0\,\sin(\theta_T)}{\sin(\theta_T - \theta_R)}, \quad (7)$$

whereas the point of intersection at the Tx is calculated as

$$\eta = \frac{x_0\,\cos(\theta_R) + y_0\,\sin(\theta_R)}{\sin(\theta_T - \theta_R)}. \quad (8)$$

If these points lie in $[-L_{T,R}/2, L_{T,R}/2]$, then the status is set to iii) or iv) respectively. Then, and after identifying which part is visible, the new center and length are calculated as

$$\begin{aligned} \eta_c &= \frac{\eta}{2} + \frac{L_T}{4} \quad or \quad \eta_c = \frac{\eta}{2} - \frac{L_T}{4} \\ l_T &= \left|\eta - \frac{L_T}{2}\right| \quad or \quad l_T = \left|\eta + \frac{L_T}{2}\right|. \end{aligned} \quad (9)$$

The same equations apply for the receiver by replacing T with R, η_c with ζ_c, and η with ζ.

IV. Calculation of the DoF

The methodology used for the calculation of the DoF is based on the eigenfunction problem initially proposed in [4] for optical systems and then in [7] for RF systems. However, the analytical solution to this problem for a generic geometric setup of two communicating surfaces is highly challenging. An alternative solution was proposed in [10] using geometric arguments and the kernel functions. The kernel function for two points ζ, ζ' on the receiving surface is given through the Green function from the point η to ζ and ζ' as

$$\begin{aligned} K_R(\zeta,\zeta') &= \int_{-l_T/2}^{l_T/2} G(\zeta,\eta)G^*(\zeta',\eta)\mathrm{d}\eta \\ &= \int_{-l_T/2}^{l_T/2} \frac{e^{-jkr}}{4\pi r}\frac{e^{jkr'}}{4\pi r'}\mathrm{d}\eta. \end{aligned} \quad (10)$$

The distance factors r, r' in the denominators may be approximated by the distance of the center of the two surfaces $d_0 = \sqrt{x_0^2 + y_0^2}$. This approximation is valid only for the amplitude and cannot be adopted for the phase terms in (10). It is easily observed that the kernel function may be written with the help of the focusing function as follows

$$\begin{aligned} K_R(\zeta,\zeta') &\approx \frac{1}{(4\pi d_0)^2}\int_{-l_T/2}^{l_T/2} e^{-j\frac{2\pi}{\lambda}(\rho-\rho')\eta}\mathrm{d}\eta \\ &= \frac{l_T}{(4\pi d_0)^2}\mathrm{sinc}\left(\frac{l_T}{\lambda}(\rho-\rho')\right), \end{aligned} \quad (11)$$

where $\mathrm{sinc}(x) = \sin(\pi x)/\pi x$. This kernel is identical to the field distribution at the receiving surface when the phase profile at the transmitting surface is set to focus towards ζ'

$$\psi(\zeta)|_{\zeta'} = \int_{-l_T/2}^{l_T/2} G(\zeta,\eta)F_T(\eta)|_{\zeta'}\mathrm{d}\eta. \quad (12)$$

In order to compute the number of the communication modes that may be supported by the two surfaces, one should calculate the number of the corresponding orthogonal steering

functions that fit within the length of the receiving surface. This is accomplished by setting a reference point ζ' and finding the number and location of the points on the receiving surface where the kernel function is zero. The usefulness of the sinc function is that one may easily calculate the points ζ where the function takes on the zero value, i.e., at integer multiples of $\frac{l_T}{\lambda}(\rho - \rho')$. Thus, assume that the reference point is at the center of the receiving surface, $\zeta' = \zeta_c$, and solve the following equation for the points ζ_m that are measured with respect to the center ζ_c and fall within the surface length, $-l_R/2 \leq \zeta_m \leq l_R/2$

$$\frac{l_T}{\lambda}(\rho_m - \rho_c) = m, \;\; m = \pm 1, \pm 2, \pm 3, ..., \tag{13}$$

where

$$\rho_m = \frac{\sin\theta_T - \gamma_m \cos\theta_T}{\sqrt{1+\gamma_m^2}} = \sin(\theta_T - a_m), \tag{14}$$

$$\gamma_m = \frac{y_0 + \zeta_c \cos\theta_R + \zeta_m \cos\theta_R - \eta_c \cos\theta_T}{x_0 - \zeta_c \sin\theta_R - \zeta_m \sin\theta_R + \eta_c \sin\theta_T}. \tag{15}$$

The parameters ρ_c, γ_c are calculated by setting $\zeta_m = 0$. This equation may be used to calculate the angles a_+, a_0, a_-. Therefore,

$$\zeta_m = \frac{\gamma_m(x_0 - \zeta_c \sin\theta_R + \eta_c \sin\theta_T) - y_0 - \zeta_c \cos\theta_R + \eta_c \cos\theta_T}{\gamma_m \sin\theta_R + \cos\theta_R}, \tag{16}$$

$$\gamma_m = \tan a_m = \tan\left(\theta_T - \arcsin\left(\rho_c + m\frac{\lambda}{l_T}\right)\right). \tag{17}$$

Substituting (17) in (16) and solving for m at $\zeta_m = \frac{l_R}{2}, \frac{-l_R}{2}$ one gets the three values m_+, m_- correspondingly

$$\begin{aligned} m_+ &= \frac{l_T}{\lambda}[\sin(\theta_T - a_+) - \rho_c], \\ m_- &= \frac{l_T}{\lambda}[\sin(\theta_T - a_-) - \rho_c], \end{aligned} \tag{18}$$

where the values of γ_+, γ_- are given by (14) setting $\zeta_m = +l_R/2, -l_R/2$ respectively. The total DoF is given by

$$m = 1 + |m_+| - |m_-|, \tag{19}$$

where the 1 has been added for the case when the Tx surface is in the far field of the receiving surface and the transmitting and receiving sides of the two surfaces are mutually visible. Equation (19) is intended as the closest integer. In Fig. 3 a typical calculation of the DoF based on (19) is given.

A. A Full Visibility Case

An interesting case is the one where $\theta_R = \pi$ and the centers of the two surfaces are aligned, i.e., $y_0 = 0$ and thus $\gamma_c = 0$. In order to maintain a full mutual visibility, i.e., $\zeta_c = \eta_c = 0$ and $l_T = L_T$, $l_R = L_R$, the rotation angle of the transmitter should lie within $[a_- - \frac{\pi}{2}, a_+ + \frac{\pi}{2}]$, while the coordinate x_0 should be positive. Setting $\zeta_m = L_R/2$ then

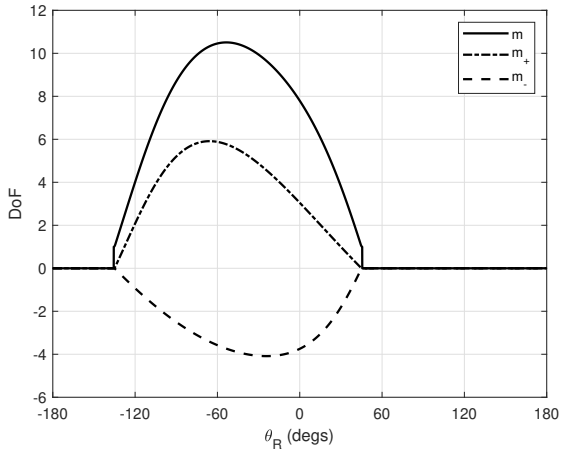

Fig. 3: The DoF for $x_0 = -5m$, $y_0 = 5m$, $L_T = 0.2m$, $L_R = 5m$, $f = 30GHz$ as given by (19).

$a_+ = \arctan\gamma_+ = \arctan(-L_R/2x_0)$ and for $\zeta_m = -L_R/2$ then $a_- = \arctan\gamma_- = \arctan(L_R/2x_0)$. Substituting in (18)

$$m_+ = \frac{L_T}{\lambda}[\sin(\theta_T - a_+) - \sin\theta_T]. \tag{20}$$

$$m_- = \frac{L_T}{\lambda}[\sin(\theta_T - a_-) - \sin\theta_T]. \tag{21}$$

The DoF are then given by

$$\begin{aligned} m &= 1 + \frac{L_T}{\lambda}[\sin(\theta_T - a_+) - \sin(\theta_T - a_-)] \\ &\overset{a_+ = -a_-}{=} 1 + \frac{2L_T}{\lambda}\cos\theta_T \sin a_-. \end{aligned} \tag{22}$$

For a very large receiving surface, i.e., for $L_R \to \infty$ and for a paraxial case, i.e., $\theta_T = 0$, $y_0 = 0$, the limit for the DoF is $\lim_{L_R\to\infty} m \approx 2L_T/\lambda$.

V. Statistical Analysis

In this section, the statistical behaviour of the achievable DoF is accurately captured under the full visibility scenario described in subsection IV.A. To this end, several key results are presented as intermediate steps in the statistical characterization of the DoF. Consider a mmWave network, where the spatial location of the center $(x_0, 0)$ of the receiving surface is modeled as a uniform binomial point process (BPP) Φ, and is uniformly and independently distributed in a finite region $\mathcal{A} \subset \mathbb{R}^2$. Without loss of generality, it is assumed that $\mathcal{A} = \mathbf{b}(\mathbf{o}, R)$, where $\mathbf{b}(\mathbf{o}, R)$ denotes a ball of radius R centered at the origin $\mathbf{o}$ and the transmitting surface is located at $\mathbf{o}$. The achievable DoF are given by (22), where $a_- = \arctan(\gamma_-)$. Notice that it is mathematically convenient to first derive the probability density function (PDF) $f_{S_-}(x)$ of the random variable $S_- = \sin a_-$ in the following Lemma.

Lemma 1. *The PDF $f_{S_-}(x)$ of the r.v. S_- is given by*

$$f_{S_-}(x) = \frac{2L_R}{\pi R^2 x^2 \sqrt{1-x^2}} \sqrt{R^2 - \left(\frac{L_R/2}{\tan(\arcsin x)}\right)^2}, \tag{23}$$

where $x \in [S_{L_R,R}, 1]$ *and* $S_{L_R,R} = \sin(\arctan(L_R/2R))$.

Proof. The conditional PDF of x_0 given that $x_0 > 0$ is given by integrating the joint PDF $f_{x_0,y_0} = 1/\pi R^2$ over y_0 as

$$f_{x_0}(x_0) = \frac{1}{\mathbb{P}[x_0 > 0]} \frac{2\sqrt{R^2 - x_0^2}}{\pi R^2}, \tag{24}$$

where $\mathbb{P}[x_0 > 0] = 1/2$ and $x_0 \in [0, R]$. Through the continuous change of variables $x_0^{'} = 1/x_0$ and subsequently $\gamma_- = \frac{L_R}{2} x_0^{'}$, the PDF of γ_- is given by

$$f_{\gamma_-}(y) = \frac{2L_R\sqrt{R^2 - \left(\frac{L_R/2}{y}\right)^2}}{\pi R^2 y^2}, \quad y \in [L_R/2R, \infty]. \tag{25}$$

Subsequently, the PDF of $a_- = \arctan \gamma_-$ can be obtained as

$$f_{a_-}(w) = \frac{2L_R \csc^2(w)}{\pi R^2 y^2}\sqrt{R^2 - \left(\frac{L_R/2}{\tan x}\right)^2}, \tag{26}$$

where $w \in [\arctan(L_R/2R), \pi/2]$. Finally, the PDF of $S_- = \sin a_-$ is given through change of variable as $f_{S_-}(x) = \frac{1}{\sqrt{1-x^2}} f_{a_-}(\arcsin x)$. The final result given by (23) results from algebraic manipulations. ∎

Now, by deriving the PDF of the function of random variable $C_{\theta_T} = \cos\theta_T$, the PDF of the product $\mathcal{P} = C_{\theta_T} \cdot S_-$ can be obtained through the formula for the product of random variables. Unfortunately, C_{θ_T} and S_- are dependent due to their common random variable a_-. In fact, θ_T is particularly tedious to work with since both its expression and its ranges are dependent on a_-. Therefore, to derive $\mathcal{P}$, the joint PDF of C_{θ_T}, S_- is obtained as an intermediate step in Lemma 2.

Lemma 2. *The joint PDF* $f_{C_{\theta_T},S_-}(c,s)$ *of the random variables* S_- *and* C_{θ_T} *is given by*

$$f_{C_{\theta_T},S_-}(c,s) = \frac{1}{\pi - 2\arcsin s} \frac{4L_R\sqrt{R^2 - \left(\frac{L_R/2}{\tan(\arcsin s)}\right)^2}}{\pi R^2 s^2 \sqrt{(1-s^2)(1-c^2)}}, \tag{27}$$

where $s \in [S_{L_R,R}, 1]$ *and* $c \in [s, 1]$.

Proof. To obtain the joint PDF of C_{θ_T} and S_-, the conditional PDF $f_{C_{\theta_T}|S_-}(c|s_0)$ should first be obtained. Recall that $\theta_T \in [\theta_T^{\min}(a_-), \theta_T^{\max}(a_-)]$, where $\theta_T^{\min}(a_-) = a_- - \frac{\pi}{2}$ and $\theta_T^{\max}(a_-) = \frac{\pi}{2} - a_-$ to ensure the visibility case described in subsection IV.A. In general, $\theta_T^{\min}(a_-)$ and $\theta_T^{\max}(a_-)$ are functions of a random variable as a consequence of a_- being a random variable. However, conditioned on $S_- = s_0 \in [S_{L_R,R}, 1]$, yields $a_- = \arcsin s_0$. Therefore, the transmitting surface is rotated by an angle θ_T, which is now uniformly and independently distributed, i.e., $\theta_T \sim U[\theta_T^{\min}(\arcsin s_0), \theta_T^{\min}(\arcsin s_0)]$. The conditional PDF $f_{\theta_T|S_-}(\theta|s_0)$ is given by

$$\begin{aligned} f_{\theta_T|S_-}(\theta|s_0) &= \frac{1}{\pi - 2\arcsin s_0} \\ &\times \mathbb{1}(\theta_T^{\min}(\arcsin s_0) \le \theta \le \theta_T^{\max}(\arcsin s_0)), \end{aligned} \tag{28}$$

where $\mathbb{1}(\cdot)$ denotes the indicator function. Next, the conditional PDF $f_{C_{\theta_T}|S_-}(c|s_0)$ is given as

$$f_{C_{\theta_T}|S_-}(c|s_0) = \frac{2f_{\theta_T|S_-}(\arccos c|s_0)}{\sqrt{1-c^2}} \mathbb{1}(s_0 \le c \le 1). \tag{29}$$

Finally, by exploiting Bayes' theorem and Lemma 1, $f_{C_{\theta_T},S_-}(c,s_0) = f_{C_{\theta_T}|S_-}(c|s_0) f_{S_-}(s_0)$. After substituting and some simplifications, Lemma 2 yields. ∎

Lemma 3. *The PDF* $f_{\mathcal{P}}(p)$ *of the random variable* $\mathcal{P}$ *is given by*

$$f_{\mathcal{P}}(p) = \begin{cases} \int_{S_{L_R,R}}^{s_{\max}(z)} \frac{1}{p} f_{C_{\theta_T},S_-}(p/s, s)\mathrm{d}s, & 0 \le p \le S_{L_R,R} \\ \int_z^{\sqrt{z}} \frac{1}{p} f_{C_{\theta_T},S_-}(p/s, s)\mathrm{d}s, & S_{L_R,R} < p < 1 \end{cases} \tag{30}$$

where $s_{\max}(z) = \max\{\sqrt{z}, S_{L_R,R}\}$.

Proof. The proof builds on the formula for the product of dependent random variables, i.e, $f_{\mathcal{P}}(p) = \int_{D_s} \frac{1}{|s|} f_{C_{\theta_T},S_-}(p/s, s)\mathrm{d}s$, where D_s denotes the range for the integration variable s. The detailed derivation of D_s is omitted here for brevity and this completes the proof. ∎

Theorem 1. *The PDF* $f_m(m)$ *of the achievable DoF* m *is given in exact form by (31) (shown at the bottom of the page) where* $\mathrm{sgn}(\cdot)$ *denotes the signum function defined as* $\mathrm{sgn}(x) = \frac{x}{|x|}$ *and* $C_{L_T,\lambda} = \frac{2L_T}{\lambda}$.

Proof. The proof follows directly from the transformation $m = C_{L_T,\lambda}\mathcal{P} + 1$ and therefore $f_m(m) = \frac{1}{C_{L_T,\lambda}} f_{\mathcal{P}}(\frac{m-1}{C_{L_T,\lambda}})$. After applying some simplifications, Theorem 1 yields. ∎

VI. Numerical Results and Discussion

In this section, numerical results are presented to evaluate the DoF achieved in a mmWave network. Similar to [10], in all presented results, the frequency, $f = 30$ GHz, the length of the transmitting surface, $L_T = 0.2m$, and the length of the receiving surface, $L_R = 2m$, are fixed. The dependency of the DoF on the distance between the two surfaces is depicted in Fig. 4, where various distances normalized to L_R are examined. The centers of the two surfaces are aligned, i.e., $y_0 = 0$, whereas $\theta_T = 0$. This result reveals the advantage

$$f_m(m) = \begin{cases} \int_{S_{L_R,R}}^{s_{\max}\left(\frac{m-1}{C_{L_T,\lambda}}\right)} \frac{1}{C_{L_T,\lambda}} \frac{L_R \,\mathrm{sgn}(s)\sqrt{4R^2 + L_R^2\left(1 - \frac{1}{s^2}\right)}}{\pi R^2 s^2 \arccos s \sqrt{(1-s^2)\left(s^2 - \left(\frac{m-1}{C_{L_T,\lambda}}\right)^2\right)}}\mathrm{d}s, & 1 \le m \le C_{L_T,\lambda} S_{L_R,R} + 1 \\ \int_{(m-1)/C_{L_T,\lambda}}^{\sqrt{(m-1)/C_{L_T,\lambda}}} \frac{1}{C_{L_T,\lambda}} \frac{L_R \,\mathrm{sgn}(s)\sqrt{4R^2 + L_R^2\left(1 - \frac{1}{s^2}\right)}}{\pi R^2 s^2 \arccos s \sqrt{(1-s^2)\left(s^2 - \left(\frac{m-1}{C_{L_T,\lambda}}\right)^2\right)}}\mathrm{d}s, & C_{L_T,\lambda} S_{L_R,R} + 1 < m < C_{L_T,\lambda} + 1, \end{cases} \tag{31}$$

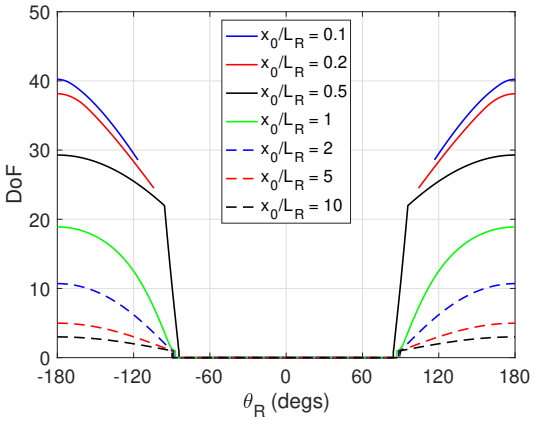

Fig. 4: The DoF for $L_T = 0.2m$, $L_R = 2m$, $f = 30GHz$, $y_0 = 0m$ and different normalized distance x_0/L_R.

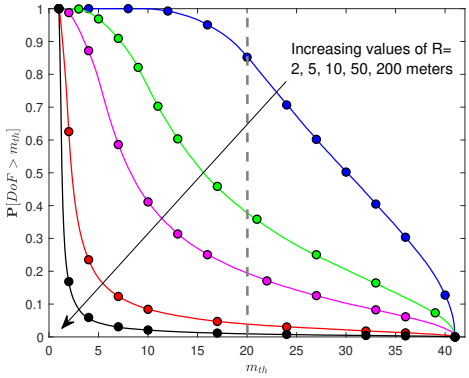

Fig. 5: cCDF of the achievable DoF versus m_{th} for different values of the radius R. Markers denote the analytical results.

provided by near-field communications in mmWave networks. Depending on the distance between the two surfaces as well as the rotation angle θ_R, the DoF takes values in the range [0,41], as expected from (22). The zero value corresponds to the case where no visibility is attained between the two surfaces.

Next, the statistical behaviour of the achievable DoF is captured and demonstrated. The accuracy of the analytical results is verified by comparison with the empirical results obtained from Monte-Carlo simulations. Fig. 5 depicts the complementary cumulative distribution function (cCDF), $F_m^c(m_{th})$, of the achievable DoF for different values of the radius R. The cCDF $F_m^c(m_{th})$ is defined as $F_m^c(m_{th}) = 1 - \mathbb{P}[m \leq m_{th}]$ and is obtained through numerical integration of Theorem 1 w.r.t the appropriate range of m. A first observation is that the probability of achieving a target value, e.g., $m_{th} = 20$ modes, which corresponds to half the maximum achievable DoF, $2L_T/\lambda$, dramatically increases with the decrease of R. In particular, as we slightly increase the value of R (starting from a small value), we notice a dramatic reduction in the DoF. This result quantifies the available DoF as the links goes from being in the near-field regime to being in the far-field regime. Not surprisingly, the curves become steepest with the increase in R. The Fraunhofer distance is $d_{FF} = 2L_R^2/\lambda = 800$ meters. Interestingly, even when $R = 200$ meters i.e, $R = \frac{1}{4}d_{FF}$, the probability that the DoF are more than 2 is hardly 20%.

VII. Conclusions

In this work, the available DoF in a wireless mmWave network with a SIS located in the near field of a LIS is examined. The proposed deterministic framework can be applied to general mmWave network deployments *beyond* the widely studied paraxial setting. To this end, apart from the length of the two surfaces, four more parameters are considered, namely the Cartesian coordinates of the center of the receiving surface and two angles that model the rotation of each surface around its center. Subsequently, a stochastic geometry framework is proposed to capture the statistical behavior of the achievable DoF available by LIS in the near field for some typical cases. Numerical results revealed: i) the advantage provided by near-field communications in mmWave networks, and ii) that for small distances between a LIS and a SIS, even small increments in the distance can drastically change the statistical behavior of the DoF and significantly reduce the achievable communications modes.

Acknowledgment

This work was co-funded by Univ. Piraeus Research Centre and the EU HORIZON programme under iSEE-6G GA No. 101139291. H. S. Dhillon gratefully acknowledges the support of US NSF (Grants ECCS-2030215 and CNS-2107276).

References

[1] C. Huang, *et al.,* "Holographic MIMO Surfaces for 6G Wireless Networks: Opportunities, Challenges, and Trends," *IEEE Wireless Commun.*, vol. 27, no. 5, pp. 118–125, Oct. 2020.

[2] D. Dardari and N. Decarli, "Holographic Communication Using Intelligent Surfaces," *IEEE Commun. Mag.* , vol. 59, no. 6, pp. 35-41, Jun. 2021.

[3] M. Di Renzo et al., "Smart Radio Environments Empowered by Reconfigurable Intelligent Surfaces: How It Works, State of Research, and The Road Ahead," *IEEE J. Sel. Areas Commun.,* vol. 38, no. 11, pp. 2450-2525, Nov. 2020.

[4] D. A. B. Miller, "Communicating with waves between volumes: Evaluating orthogonal spatial channels and limits on coupling strengths", *Appl. Opt.,* vol. 39, no. 11, pp. 1681-1699, Apr. 2000.

[5] M. Franceschetti, "*Wave Theory of Information*", Cambridge Univ. Press, 2018.

[6] A. Pizzo, T. L. Marzetta and L. Sanguinetti, "Degrees of Freedom of Holographic MIMO Channels," in *Proc. IEEE 21st Int. Workshop Signal Process. Adv. Wireless Commun. (SPAWC)*, May 2020, pp. 1–5.

[7] D. Dardari, "Communicating With Large Intelligent Surfaces: Fundamental Limits and Models", *IEEE J. Sel. Areas Commun.,* vol. 38, no. 11, pp. 2526-2537, Nov. 2020.

[8] Y. Liu, Z. Wang, J. Xu, C. Ouyang, X. Mu and R. Schober, "Near-Field Communications: A Tutorial Review" *IEEE Open J. Commun. Soc.,* vol. 4, pp. 1999-2049, Aug. 2023.

[9] H. Zhang, N. Shlezinger, F. Guidi, D. Dardari and Y. C. Eldar, "6G Wireless Communications: From Far-Field Beam Steering to Near-Field Beam Focusing," *IEEE Commun. Mag.,* vol. 61, no. 4, pp. 72-77, Apr. 2023.

[10] N. Decarli and D. Dardari, "Communication Modes With Large Intelligent Surfaces in the Near Field," *IEEE Access,* vol. 9, pp. 165648–165666, Dec. 2021.